Proceedings of the Seventeenth International Conference on
Civil, Structural and Environmental Engineering Computing
Edited by: P. Iványi, J. Kruis and B.H.V. Topping
Civil-Comp Conferences, Volume 6, Paper 14.2
Civil-Comp Press, Edinburgh, United Kingdom, 2023
doi: 10.4203/ccc.6.14.2

An Efficient Quadrilateral Element based on the Discrete Shear Projection Method and Free Formulation

A.M. Katili and I. Katili

Department of Civil Engineering, University of Indonesia, Depok, Indonesia

Abstract

This paper presents the enhancement of a previously developed linear quadrilateral plate element by using incomplete quadratic functions. As in the free formulation concept, the couple bending energy between lower (linear) and higher (quadratic) modes is forced to be zero in order to satisfy the constant bending patch test. The discrete shear projection method (DSPM) is used to define the independent transverse shear strains and avoid the shear locking phenomenon. The improved quadrilateral element has four nodes and 3 degrees of freedom (DOFs) per node. It is free of shear locking, has a proper rank, and passes the bending moment patch tests. The application in static analysis exhibits excellent convergence behaviour, reliability, and precision.

Keywords: Reissner-Mindlin, plate, quadrilateral element, discrete shear projection, free formulation, linear analysis, patch-test, shear locking.

1 Introduction

When using a four-node quadrilateral finite element with a total of 12 DOFs, it is crucial to have a reliable element for a wide range of slenderness ratios (such as $10^4 \leq L/h \leq 4$). Among the characteristics that must be possessed are not showing shear locking and passing the constant bending moment patch tests. As a response to the issue, a selective numerical integration with special schemes for shear strains proposed by MacNeal (1982) [1] has been highly suggested in preventing shear locking. But this technique works only for rectangular elements and not for quadrilateral elements.

Starting with Reissner-Mindlin (RM) plate theory, in 1982, Batoz and Ben Tahar devised a quadrilateral element named Discrete Kirchhoff Quadrilateral (DKQ) [2] using discrete side constraints to disregard transverse shear energy. This 12 DOF element has four corner nodes, each with 3 DOFs. Due to its nature, the element only applies to thin plates.

Using a modified RM plate theory and C^1 continuity, Bergan and Wang 1984 [3] develop a quadrilateral element based on the energy-orthogonal free formulation approach. The transverse displacement w is the only independent variable, the curvatures $\{\chi\}$ is expressed as the second and fourth derivatives of w, and the transverse shear strains $\{\gamma\}$ is expressed as the third derivative of w. The convergence behaviour of this element is excellent for thin to moderately thick plates. For a very thick plate, the accuracy of this element is slightly decreased.

Dvorkin and Bathe (1984) [4] and Bathe and Dvorkin (1985) [5] introduced the Mixed Interpolation of Tensorial Components (MITC4) element, a simple formulation with 12 DOFs which takes into account transverse shear effects.

Katili (1993) [6] introduced the Discrete Kirchhoff Mindlin Quadrilateral (DKMQ) element as an improvement of the DKQ element. It uses discrete constraints to account for transverse shear effects and normal tangential incomplete equilibrium equations along the sides of the element to get constant transverse shear strains. The DKMQ is suitable for plates with thicknesses ranging from thin to thick, free of shear locking, possesses excellent convergence properties, and passes patch tests.

Ko et al. (2016, 2017a, 2017b) [7-9] improved MITC4 to MITC4+ plate and shell element, which shows excellent performance on selected shell benchmark tests.

Katili et al. (2021) and (2023) [10-11] recently presented a simple quadrilateral element referred to as Q4γ_s based on the DSPM (discrete shear projection method) for functionally graded materials (FGM) plates.

This paper aims to improve the Q4γ_s [10-11] element using incomplete quadratic functions for rotations and the free formulation method of Bergan and Wang [3]. The new quadrilateral plate element called Q4γ_s+ is the paper's primary contribution. It has four nodes and three DOFs per node (transverse displacement w and two rotations, i.e. β_x in the z-x plane and β_y in the z-y plane).

2 Formulation of Q4γ_s+ element

2.1 Displacement functions

The transverse displacement w is expressed using bilinear shape functions as in Equation (1). Meanwhile, the rotations β_x and β_y at four corner nodes (Figure 1) are interpolated with a bilinear shape functions N_i (i = 1,2,3,4) as in Equation (2). The four temporary DOFs of $\Delta\beta_{s_k}$ (k = 5,6,7,8) at all sides are interpolated using incomplete quadratic functions to enhance Q4γ_s. The displacement *w*, rotation function β_x, and rotation function β_y of the Q4γ_s+ element can be written as:

$$w = \sum_{i=1}^{4} N_i w_i \tag{1}$$

$$\beta_x = \sum_{i=1}^{4} N_i \beta_{x_i} + \sum_{k=5}^{8} P_k C_k \Delta\beta_{s_k} \quad ; \quad \beta_y = \sum_{i=1}^{4} N_i \beta_{y_i} + \sum_{k=5}^{8} P_k S_k \Delta\beta_{s_k} \tag{2}$$

The bilinear shape functions N_i as the lower order shape functions as in Equation (3) and the incomplete quadratic functions P_k as the higher order shape functions are given by Equation (4).

$$\begin{aligned} N_1 &= \frac{1}{4}(1-\xi)(1-\eta) \ ; \ N_2 = \frac{1}{4}(1+\xi)(1-\eta) \\ N_3 &= \frac{1}{4}(1+\xi)(1+\eta) \ ; \ N_4 = \frac{1}{4}(1-\xi)(1+\eta) \end{aligned} \tag{3}$$

$$\begin{aligned} P_5 &= \frac{1}{2}\left(1-\xi^2\right)(1-\eta) \ ; \ P_6 = \frac{1}{2}(1+\xi)\left(1-\eta^2\right) \\ P_7 &= \frac{1}{2}\left(1-\xi^2\right)(1+\eta) \ ; \ P_8 = \frac{1}{2}(1-\xi)\left(1-\eta^2\right) \end{aligned} \tag{4}$$

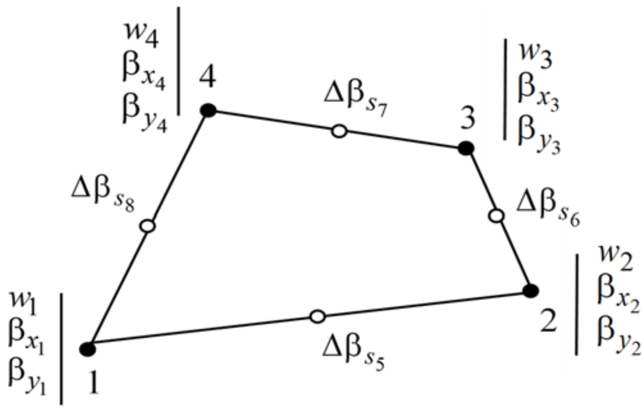

Figure 1: Q4γ_s+ element with 3 DOFs at corner nodes and four temporary DOFs at mid-sides.

2.2 Curvatures and bending energy

By using Equation (2), the bending strain matrix will comprise two parts, i.e., lower and higher order.

$$\{\chi\} = \begin{Bmatrix} \chi_x \\ \chi_y \\ \chi_{xy} \end{Bmatrix} = \begin{Bmatrix} \beta_{x},_{x} \\ \beta_{y},_{y} \\ \beta_{x},_{y} + \beta_{y},_{x} \end{Bmatrix} = \left[B_{b_u}\right]\{u_n\} + \left[B_{b_\Delta}\right]\{\Delta\beta_n\}$$
$$\langle u_n \rangle = \langle \ldots \quad w_i \quad \beta_{x_i} \quad \beta_{y_i} \quad \cdots \rangle_{i=1,4} \tag{5}$$

$$\langle \Delta\beta_n \rangle = \langle \Delta\beta_{s_5} \quad \Delta\beta_{s_6} \quad \Delta\beta_{s_7} \quad \Delta\beta_{s_8} \rangle$$

where the lower order of the bending strain matrix is

$$\left[B_{b_u}\right] = \begin{bmatrix} & 0 & N_{i,x} & 0 & & \\ \dots & 0 & 0 & N_{i,y} & \dots & i=1,4 \\ & 0 & N_{i,y} & N_{i,x} & & \end{bmatrix} \; ; \quad \begin{matrix} N_{i,x} = j_{11} N_{i,\xi} + j_{12} N_{i,\eta} \\ N_{i,y} = j_{21} N_{i,\xi} + j_{22} N_{i,\eta} \end{matrix} \tag{6}$$

and the higher order of the bending strain matrix is

$$\left[B_b^h\right] = \begin{bmatrix} & P_{k,x} C_k & & \\ \dots & P_{k,y} S_k & \dots & k=5,8 \\ & P_{k,y} C_k + P_{k,x} S_k & & \end{bmatrix} \; ; \quad \begin{matrix} P_{k,x} = j_{11} P_{k,\xi} + j_{12} P_{k,\eta} \\ P_{k,y} = j_{21} P_{k,\xi} + j_{22} P_{k,\eta} \end{matrix} \tag{7}$$

with j_{11}, j_{12}, j_{21}, and j_{22} are the terms of the Jacobian matrix inverse. C_k and S_k are the directional cosines of side k (Figure 2).

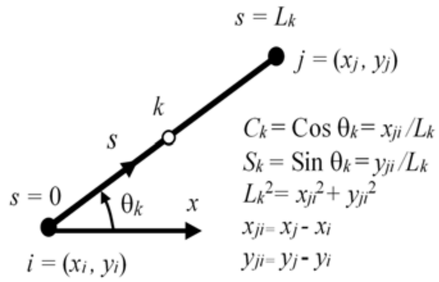

i	j	k
1	2	5
2	3	6
3	4	7
4	1	8

Figure 2: The side k direction cosines.

The bending energy of Q4γ_s+ can be represented as follows:

$$\Pi_{\text{int}}^b = \frac{1}{2}\int_A \langle\chi\rangle\left[H_b\right]\{\chi\}\, dA \; ; \; \left[H_b\right] = D_b \begin{bmatrix} 1 & \upsilon & 0 \\ \upsilon & 1 & 0 \\ 0 & 0 & (1-\upsilon)/2 \end{bmatrix} \; ; \; D_b = \frac{Eh^3}{12\left(1-\upsilon^2\right)} \tag{8}$$

$\left[H_b\right]$ is the bending rigidity matrix, E is the modulus elasticity, h is the plate thickness, and υ is the Poison ratio.

We assumed the zero coupling bending energy to fulfil the constant bending patch test [3]. By introducing Equation (5-7) into Equation (8), the bending energy in Equation (8) can be rewritten as follows:

$$\Pi_{\text{int}}^b = \frac{1}{2}\langle u_n\rangle\left[k_{b_u}\right]\{u_n\} + \frac{1}{2}\langle\Delta\beta_n\rangle\left[k_{b_\Delta}\right]\{\Delta\beta_n\} \tag{9}$$

where the lower order and higher bending stiffness are

$$\left[k_{b_u}\right] = \int_A \left[B_{b_u}\right]^T \left[H_b\right]\left[B_{b_u}\right] dA \tag{10}$$

$$\left[k_{b_\Delta}\right] = \int_A \left[B_{b_\Delta}\right]^T \left[H_b\right]\left[B_{b_\Delta}\right] dA$$

2.3 Discrete shear projection method

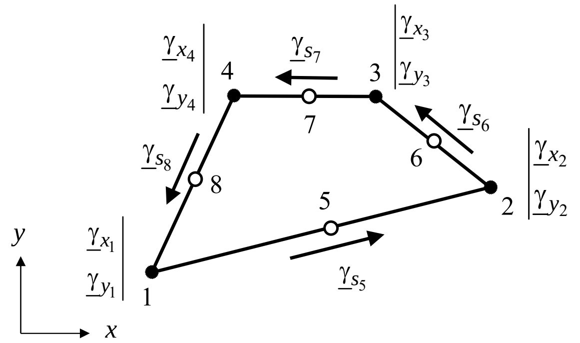

i	k	m
1	5	8
2	6	5
3	7	6
4	8	7

Figure 3: Shear strains at node *i* and constant shear strains on four sides of the element.

The transverse shear strain in the tangential *s*-direction can be expressed as:

$$\gamma_{s_k} = \frac{w_j - w_i}{L_k} + \left(1 - \frac{s}{L_k}\right)\beta_{s_i} + \frac{s}{L_k}\beta_{s_j} + 4\frac{s}{L_k}\left(1 - \frac{s}{L_k}\right)\Delta\beta_{s_k} \tag{11}$$

Assuming that the shear strains on the side are constant, we have the following:

$$\underline{\gamma}_{s_k} = \frac{1}{L_k}\int_0^{L_k} \gamma_{s_k}\, ds \tag{12}$$

Substituting Equation (11) into Equation (12) and with Figure 2, we obtain:

$$\underline{\gamma}_{s_k} = \frac{w_j - w_i}{L_k} + \frac{1}{2}\left(C_k\beta_{x_i} + S_k\beta_{y_i} + C_k\beta_{x_j} + S_k\beta_{y_j}\right) + \frac{2}{3}\Delta\beta_{s_k} \tag{13}$$

Using constitutive and incomplete equilibrium equations in local normal-tangential (*n*-*s*) coordinates on each side *k* (*i*-*j*), in [6], Katili proposed the independent transverse shear strain as follows:

$$\underline{\gamma}_{s_k} = -\frac{2}{3}\phi_k \Delta\beta_{s_k} \quad ; \quad \phi_k = \frac{2}{\kappa(1-\upsilon)}\left(\frac{h^2}{L_k^2}\right) \tag{14}$$

where κ is the shear correction factor.

Substituting Equation (14) into Equation (13) and applying it to the four sides of an element gives

$$\left\{\Delta\beta_n\right\} = \left[\phi_\Delta\right]\left[A_u\right]\left\{u_n\right\} \tag{15}$$

$$[\phi_\Delta] = -\frac{3}{2}\begin{bmatrix} \frac{1}{(1+\phi_5)} & 0 & 0 & 0 \\ 0 & \frac{1}{(1+\phi_6)} & 0 & 0 \\ 0 & 0 & \frac{1}{(1+\phi_7)} & 0 \\ 0 & 0 & 0 & \frac{1}{(1+\phi_8)} \end{bmatrix} \tag{16}$$

$$[A_u] = \frac{1}{2}\begin{bmatrix} -\frac{2}{L_5} & C_5 & S_5 & \frac{2}{L_5} & C_5 & S_5 & 0 & 0 & 0 & 0 & 0 & 0 \\ 0 & 0 & 0 & -\frac{2}{L_6} & C_6 & S_6 & \frac{2}{L_6} & C_6 & S_6 & 0 & 0 & 0 \\ 0 & 0 & 0 & 0 & 0 & 0 & -\frac{2}{L_7} & C_7 & S_7 & \frac{2}{L_7} & C_7 & S_7 \\ \frac{2}{L_8} & C_8 & S_8 & 0 & 0 & 0 & 0 & 0 & 0 & -\frac{2}{L_8} & C_8 & S_8 \end{bmatrix} \tag{17}$$

Applying Equation (14) to the four sides of an element yields

$$\begin{Bmatrix} \underline{\gamma}_{s_5} \\ \underline{\gamma}_{s_6} \\ \underline{\gamma}_{s_7} \\ \underline{\gamma}_{s_8} \end{Bmatrix} = -\frac{2}{3}\begin{bmatrix} \phi_5 & 0 & 0 & 0 \\ 0 & \phi_6 & 0 & 0 \\ 0 & 0 & \phi_7 & 0 \\ 0 & 0 & 0 & \phi_8 \end{bmatrix}\begin{Bmatrix} \Delta\beta_{s_5} \\ \Delta\beta_{s_6} \\ \Delta\beta_{s_7} \\ \Delta\beta_{s_8} \end{Bmatrix} \tag{18}$$

The relationship between the constant shear strains on the four sides and the temporary DOFs in Equation (18) can be rewritten in the compact form as follows:

$$\{\underline{\gamma}_n\} = [\phi_\gamma]\{\Delta\beta_n\} \tag{19}$$

Substituting Equation (15) into Equation (19), we have:

$$\{\underline{\gamma}_n\} = [\phi_{\gamma\Delta}][A_u]\{u_n\} \tag{20}$$

where:

$$[\phi_{\gamma\Delta}] = \begin{bmatrix} \frac{\phi_5}{(1+\phi_5)} & 0 & 0 & 0 \\ 0 & \frac{\phi_6}{(1+\phi_6)} & 0 & 0 \\ 0 & 0 & \frac{\phi_7}{(1+\phi_7)} & 0 \\ 0 & 0 & 0 & \frac{\phi_8}{(1+\phi_8)} \end{bmatrix} \tag{21}$$

The shear strains at node *i* are calculated by projecting the constant shear strains on the two sides sharing node *i*. From Figure 3, the shear strains at node *i* are determined as follows [10-11]:

$$\begin{Bmatrix} \underline{\gamma}_{x_i} \\ \underline{\gamma}_{y_i} \end{Bmatrix} = \frac{1}{A_i} \begin{bmatrix} S_m & -S_k \\ -C_m & C_k \end{bmatrix} \begin{Bmatrix} \underline{\gamma}_{s_k} \\ \underline{\gamma}_{s_m} \end{Bmatrix} ; A_i = C_k S_m - C_m S_k \quad (22)$$

C_k, S_k, C_m, and S_m are the directional cosines of sides *k* and *m* (Figure 3) that share the same corner node *i*.

The independent shear strains $\langle \underline{\gamma}_x \quad \underline{\gamma}_y \rangle$ are associated with shear strains on four nodes as follows (Figure 3):

$$\{\underline{\gamma}\} = \begin{Bmatrix} \underline{\gamma}_x \\ \underline{\gamma}_y \end{Bmatrix} = \sum_i^4 N_i \begin{Bmatrix} \underline{\gamma}_{x_i} \\ \underline{\gamma}_{y_i} \end{Bmatrix} \quad (23)$$

By substituting Equation (22) into Equation (23), the independent shear strains can be expressed in the following form:

$$\{\underline{\gamma}\} = \begin{Bmatrix} \underline{\gamma}_x \\ \underline{\gamma}_y \end{Bmatrix} = \left[B_{s_\gamma} \right] \{\underline{\gamma}_n\} \; ; \; \langle \underline{\gamma}_n \rangle = \langle \underline{\gamma}_{s_5} \quad \underline{\gamma}_{s_6} \quad \underline{\gamma}_{s_7} \quad \underline{\gamma}_{s_8} \rangle \quad (24)$$

where:

$$\left[B_{s_\gamma} \right] = \left[\left[B_{s_{\gamma 1}} \right] \; \left[B_{s_{\gamma 2}} \right] \; \left[B_{s_{\gamma 3}} \right] \; \left[B_{s_{\gamma 4}} \right] \right]$$

$$\left[B_{s_{\gamma 1}} \right] = \begin{bmatrix} \left(\frac{S_8}{A_1} N_1 - \frac{S_6}{A_2} N_2 \right) \\ \left(\frac{C_6}{A_2} N_2 - \frac{C_8}{A_1} N_1 \right) \end{bmatrix} ; \left[B_{s_{\gamma 2}} \right] = \begin{bmatrix} \left(\frac{S_5}{A_2} N_2 - \frac{S_7}{A_3} N_3 \right) \\ \left(\frac{C_7}{A_3} N_3 - \frac{C_5}{A_2} N_2 \right) \end{bmatrix} \quad (25)$$

$$\left[B_{s_{\gamma 3}} \right] = \begin{bmatrix} \left(\frac{S_6}{A_3} N_3 - \frac{S_8}{A_4} N_4 \right) \\ \left(\frac{C_8}{A_4} N_4 - \frac{C_6}{A_3} N_3 \right) \end{bmatrix} ; \left[B_{s_{\gamma 4}} \right] = \begin{bmatrix} \left(\frac{S_7}{A_4} N_4 - \frac{S_5}{A_1} N_1 \right) \\ \left(\frac{C_5}{A_1} N_1 - \frac{C_7}{A_4} N_4 \right) \end{bmatrix}$$

Substituting Equation (20) into Equation (24) leads to

$$\{\underline{\gamma}\} = [B_s]\{u_n\} \; ; \; [B_s] = \left[B_{s_\gamma} \right] \left[\phi_{\gamma\Delta} \right] [A_u] \quad (26)$$

2.4 Bending and shear stiffness

Substituting Equation (15) into Equation (9), we obtain

$$\Pi_{int}^b = \frac{1}{2} \langle u_n \rangle [k_b] \{u_n\} \quad (27)$$

where the bending stiffness matrix is

$$[k_b] = \left[k_{b_u} \right] + [A_u]^T [\phi_\Delta]^T \left[k_{b_\Delta} \right] [\phi_\Delta] [A_u] \quad (28)$$

The shear strain energy can be calculated using the following:

$$\Pi_{\text{int}}^{s} = \frac{1}{2}\int_A \langle \underline{\gamma} \rangle [H_s] \{\underline{\gamma}\} \; dA \tag{29}$$

where $[H_s]$ is the transverse shear rigidity matrix as follows:

$$[H_s] = D_s \begin{bmatrix} 1 & 0 \\ 0 & 1 \end{bmatrix} \;;\; D_s = \kappa G h \;;\; G = \frac{E}{2(1+\upsilon)} \tag{30}$$

Substituting Equation (26) into Equation (29), we have the shear energy as follows:

$$\Pi_{\text{int}}^{s} = \frac{1}{2}\langle u_n \rangle [k_s] \{u_n\} \tag{31}$$

where the shear stiffness matrix is

$$[k_s] = \int_A [B_s]^T [H_s][B_s] dA \tag{32}$$

Finally, the total stiffness is:

$$[k] = [k_b] + [k_s] \tag{33}$$

3 Results of Razzaque's skew plate

This skew plate of 60° (Figure 4) subjected to a uniformly distributed load $f_z = 1$ was originally evaluated by Razzaque (1973). This structure has hard simply supported on *AB* and *CD* and free on *AD* and *BC*. Each side of this plate has a length of $L = 1000$. In this paper, the Razzaque's plate was analyzed with different meshes $N \times N$ with $N =$ 4, 8, 16, 24, 32, 48, and 64.

The solution of Razzaque's skew plate ($E = 1085$, $\upsilon = 0.31$) is [12]:

Central displacement : $w_c = 7.945 \times 10^{-3} f_z L^4/D_b$

Central moment : $M_y = 95.89 \times 10^{-3} f_z L^2$

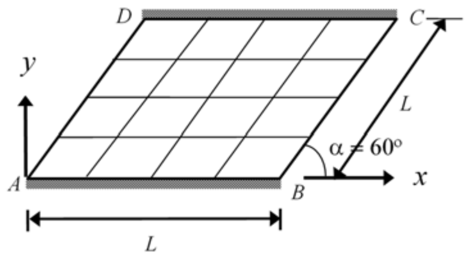

Figure 4: Razzaque 60° skew plate with 4×4 mesh.

Figure 5 shows the non-dimensional central displacements $\underline{w_c}$ and moments $\underline{M_y}$ of the Razzaque's plate [12] for $L/h = 1000$ and $L/h = 5$. For $L/h = 5$, we use the DKMQ [6] element with 64×64 mesh as a reference. We can observe that the Q4γ_s+ converges faster than Q4γ_s [10-11].

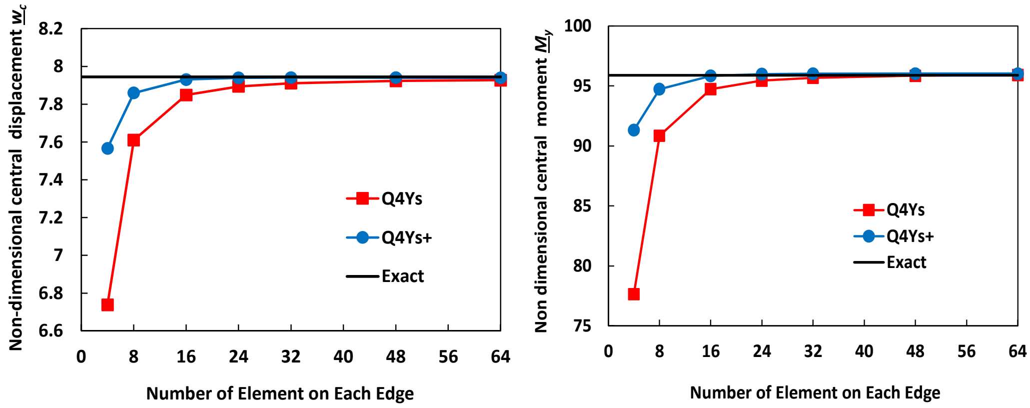

Figure 5: Convergence rate of Razzaque's plate (L/h =1000).

4 Conclusions and Contributions

The new Q4γ_s+ element has been developed using the discrete shear projection method to prevent the occurrence of shear-locking. In the Q4γ_s+ formulation, the bilinear shape functions of rotation β_x in the z-x plane and β_y in the z-y plane are enriched with incomplete quadratic functions. As in the free formulation concept, the coupling bending energy between lower and higher bending energy is assumed to be zero, which makes the element pass the constant bending patch test. The results indicate that Q4γ_s+ is simple, efficient, has the correct rank, and is applicable for thin to thick plates.

Acknowledgements

We gratefully acknowledge the financial support provided by Universitas Indonesia through the PUTI-Q1 2023 Scheme programme (Contract No. NKB-518/UN2.RST/ HKP.05.00/2023).

References

[1] R.H. MacNeal, "Derivation of element stiffness matrices by assumed strain distributions", Nuclear Engineering and Design, 70, 3-12, 1982. https://doi.org/ 10.1016/0029-5493(82)90262-X

[2] J.L. Batoz, M. Ben Tahar, "Evaluation of a new thin plate quadrilateral element", International Journal for Numerical Methods in Engineering, 18, 1655-1678, 1982. https://doi.org/10.1002/nme.1620181106

[3] P.G. Bergan, X. Wang, "Quadrilateral plate bending elements with shear deformations", Computer and Structures, 19, 25–34, 1984. https://doi.org/ 10.1016/0045-7949(84)90199-8

[4] E.N. Dvorkin, K.J. Bathe, "A continuum mechanics based four-node shell element for general non-linear analysis". Engineering computations, 1, 77-88, 1984. http://dx.doi.org/10.1108/eb023562

[5] K.J. Bathe, E.N. Dvorkin, "A four-node plate bending element based on Mindlin-Reissner plate theory and a mixed interpolation", International Journal for Numerical Methods in Engineering, 21, 367-383, 1985.

https://doi.org/ 10.1002/nme.1620210213
[6] I. Katili, "A new discrete Kirchhoff-Mindlin element based on Mindlin-Reissner plate theory and assumed shear strain fields- part II: An extended DKQ element for thick plate bending analysis". International Journal for Numerical Methods in Engineering, 36, 1885-1908, 1993. https://doi.org/10.1002/NME. 1620361107
[7] Y. Ko, P.S. Lee, K.J. Bathe, "The MITC4+ shell elements and its performance", Computers and Structures, 169, 57–68, 2016. http://dx.doi.org/10.1016/ j.compstruc.2016.03.002
[8] Y. Ko, P.S. Lee, K.J. Bathe, "A new MITC4+ shell element", Computers and Structures, 182, 404-418, 2017. http://dx.doi.org/10.1016/j.compstruc.2016. 11.004
[9] Y. Ko, P.S. Lee, K.J. Bathe, "The MITC4+ shell element in geometric nonlinear analysis", Computer and Structures, 185, 1-14, 2017. http://dx.doi.org/10.1016/ j.compstruc.2017.01.015
[10] I. Katili, J.L. Batoz, I.J. Maknun, A.M. Katili, "On static and free vibration analysis of FGM plates using an efficient quadrilateral finite element based on DSPM", Composite Structures, 261, 113514, 2021. https://doi.org/10.1016/ j.compstruct.2020.113514
[11] I. Katili, J.L. Batoz, S. Bouabdallah, I.J. Maknun, A.M. Katili, "Discrete shear projection method for mechanical buckling analysis of FGM sandwich plates", Composite Structures, 312, 116825, 2023. https://doi.org/10.1016/j.compstruct. 2023.116825
[12] A. Razzaque, "Program for triangular bending elements with derivative smoothing", Int. J. Numer. Meth. Eng., 6, 333-345, 1973. https://doi.org/10.1002/ nme.1620060305